Nuclear Science and Techniques (2026) 37:114
https://doi.org/10.1007/s41365-026-01946-x

A neural network approach for two-body systems with spin and isospin degrees of freedom

Chuan-Xin Wang[1,2] · Tomoya Naito[2,3,4] · Jian Li[1] · Hao-Zhao Liang[2,4]

Received: 22 August 2025 / Revised: 7 November 2025 / Accepted: 14 December 2025 / Published online: 10 April 2026

Abstract
We propose an enhanced machine learning method to calculate the ground state of two-body systems. By extending the original method [Phys. Rev. Res. **5**, 033189 (2023)], the present method enables consideration of the spin and isospin degrees of freedom by employing a non-fully connected deep neural network and unsupervised machine learning technique. The validity of this method is verified by calculating the unique bound state of the deuteron.

Keywords Nuclear structure · Unsupervised machine learning · Deep neural network · Deuteron

1 Introduction

Quantum systems, from atomic nuclei to solids, are composed of many particles; thus, finding the states of many-body systems is an essential problem. In advanced quantum many-body methods, such as density functional theory [1–3], tensor network [4, 5], and variational Monte Carlo method [6–8], the ground-state energy can be treated in a variational form, turning finding the ground state of the system into a variational problem. Among the methods for solving the variational problems, unsupervised machine learning (ML) is gaining attention owing to its powerful performance for optimization, making it an ideal tool for solving many-body problems in quantum systems.

In unsupervised ML for variational problems, the ML structure can be treated as a trial function. In the case of quantum many-body systems, the energy expectation value $\langle H \rangle$ with respect to the system Hamiltonian H is treated as the loss function, and the output of the ML is usually regarded as the wave function.

For unsupervised ML applications in spin systems, restricted Boltzmann machines (RBMs) were first employed as a wave function ansatz to address both static and time-evolution problems [9]. Subsequently, improved algorithms were developed to enhance accuracy [10], and deterministic time-evolution schemes were introduced [11]. Additionally,

T.N. acknowledges the JSPS Grant-in-Aid for Transformative Research Areas (A) under Grant No. JP25H01558, the JSPS Grant-in-Aid for Scientific Research (S) under Grant No. JP25H00402, the JSPS Grant-in-Aid for Scientific Research (B) under Grant Nos. JP23K26538 and JP25K01003, the JSPS Grant-in-Aid for Scientific Research (C) under Grant No. JP23K03426, the JSPS Grant-in-Aid for Early-Career Scientists under Grant No. JP24K17057, the JSPS Grant-in-Aid for JSPS Fellows under Grant No. JP25KJ0405, and JST COI-NEXT Grant No. JPMJPF2221. J.L. acknowledges the National Natural Science Foundation of China (Nos. 12475119 and 11675063) and the Key Laboratory of Nuclear Data Foundation (No. JCKY2025201C154). H.L. acknowledges the JSPS Grant-in-Aid for Scientific Research (S) under Grant No. JP20H05648 and the RIKEN Pioneering Project: Evolution of Matter in the Universe. The numerical calculations were performed on cluster computers at the RIKEN iTHEMS Center.

✉ Tomoya Naito
tnaito@ribf.riken.jp

✉ Jian Li
jianli@jlu.edu.cn

✉ Hao-Zhao Liang
haozhao.liang@phys.s.u-tokyo.ac.jp

[1] College of Physics, Jilin University, Changchun 130012, China

[2] RIKEN Center for Interdisciplinary Theoretical and Mathematical Sciences (iTHEMS), Wako 351-0198, Japan

[3] Department of Nuclear Engineering and Management, Graduate School of Engineering, The University of Tokyo, Tokyo 113-8656, Japan

[4] Department of Physics, Graduate School of Science, The University of Tokyo, Tokyo 113-0033, Japan

the Jastrow–Slater wave function ansatz was adapted for unsupervised ML [12]. The excited-state calculation was presented with two different ansätze [13, 14].

In the field of nuclear physics, ML has emerged as a crucial tool with extensive and impactful applications [15, 16]. These applications span the prediction of both nuclear ground- and excited-state properties, including nuclear mass [17–21], charge radius [22, 23], excited states [24, 25], α decay [26, 27], β decay [28, 29], charge density [30–32], density functional [33], nuclear level density [34, 35], ground-state magnetic moments [36], photoabsorption cross section [37], single-Λ hypernuclei [38], and the distribution of ground-state spin in the two-body random ensemble [39]. In statistical mechanics, the transfer matrix for a spin-glass model was calculated using an unsupervised deep neural network [40].

For many-body systems of bosons or fermions depending on continuous coordinates, incorporating the required (anti) symmetrization into the neural network wave function presents a significant challenge. In Ref. [41], a single-layer neural network was used to calculate deuterons in the momentum space with a pre-training process. In Ref. [42], further analysis was conducted on the structure of neural networks and numerical uncertainty. For bosonic systems, Ref. [43] introduced a neural network wave function for studying the Calogero-Sutherland model and Efimov bound states, while Ref. [44] proposed incorporating a pooling layer to enforce symmetrization. For fermionic systems, such as electronic structure of atoms and molecules and nuclear structure with an *ab initio* Hamiltonian, the Jastrow-Slater ansatz is often introduced to consider the fermion antisymmetrization and the interparticle correlation [45–51]. The hidden-fermion technique [52], which is an extension of the Jastrow–Slater ansatz, was proposed and applied with an unsupervised ML. This technique was immediately applied to nuclear systems to search for the ground-state energy of ^{16}O [53], and both energies and other ground-state properties of $A \leq 20$ nuclei [54]. Another proposed method for calculating the electronic structure is to map the fermionic system into a spin system [55]. Recent progress is summarized in Ref. [56].

Among these methods, in Ref. [44], bosonic symmetrization is considered using the pooling layer, whereas it does not work for fermionic systems. A Jastrow-Slater wave function is applied in many works to solve fermionic systems [45–51]; however, it does not work for bosonic systems.

In Ref. [57], another method using an unsupervised deep neural network (DNN) was proposed, which can solve both bosonic and fermionic systems in coordinate space. The calculation steps are the same for both bosonic and fermionic systems, differing only in the sign in the trial wave function to account for (anti)symmetrization. According to the universal approximation theorem [58, 59], a multilayer neural network can approximate any function with the desired accuracy by changing the size of the neural network. Therefore, a neural network can be used as a trial wave function [9–11, 41–43, 56, 57]. By utilizing the energy expectation as the loss function for minimization, this method successfully calculated the ground state of one-dimensional (1D) one- to three-body systems. However, the spin and isospin degrees of freedom, which are crucial for discussing the properties of magnetic materials and atomic nuclei, have not yet been considered in this method. [1]

In this study, we extend the method proposed in Ref. [57] to include spin and isospin degrees of freedom. We will focus on two-body systems without external potential as the first step. Owing to translational symmetry, only the relative motion was considered. This setup corresponds to the one-body calculation in Ref. [57]. This method is validated by calculating the deuteron, the simplest realistic many-body system. Its Hamiltonian contains a noncentral tensor force, making the inclusion of spin and isospin degrees of freedom essential. Because a deuteron has only one bound state, we do not focus on the excited states in the present discussion.

Note that the system we consider is the same as that in Refs. [41, 42]. However, our method is technically different from theirs. In the process of optimization, Ref. [41] used a supervised method to pre-train DNN parameters, facilitating faster convergence and ensuring accurate behavior at the origin [42, 60]. Our method does not require pre-training, primarily because of the choice of the DNN ansatz for the wave functions. This choice influences the behavior at the origin (discussed in the Appendix), along with other technical differences, such as mesh point distributions and optimizers. It was pointed out in Ref. [42] that the structure of a neural network affects the convergence, where a deeper neural network yields a lower convergence rate. In contrast, our DNN model always converges with different numbers of layers by ensuring a relatively smaller number of hidden nodes. In the results, overfitting is not observed in our DNN wave functions, whereas it appeared in Ref. [42]. In Ref. [41], it was also pointed out that the extension to arbitrary spin and isospin was a future perspective; our work derived a general formula for arbitrary spin and isospin and calculated the deuteron with 18 possible partial waves by applying a non-fully connected DNN structure.

The remaining of this paper is organized as follows. In Sect. 2, we discuss the theory to include the spin and isospin degrees of freedom. The corresponding DNN model is proposed in Sect. 3. In Sect. 4, we discuss the calculation results of the deuteron. Finally, we provide a summary and future perspectives in Sect. 5.

[1] It should be noted that the spin and isospin degrees of freedom have been taken into account for machine learning calculation with the Jastrow–Slater ansatz in, e.g., Refs. [47–51, 53].

2 Method

2.1 Hamiltonian for two-body systems with spin and isospin degrees of freedom

A general self-bound two-body system is studied with the Hamiltonian expressed in coordinate space as

$$H = -\frac{\hbar^2}{2m_1}\nabla_1^2 - \frac{\hbar^2}{2m_2}\nabla_2^2 + V^{\text{int}}(\boldsymbol{r}_1, \boldsymbol{r}_2), \tag{1}$$

where ∇^2 denotes the Laplacian and V^{int} denotes the two-body interaction. Since we consider a self-bound system, which has a translational symmetry, the center-of-mass motion can be isolated. Hence, only the relative motion is considered in the following calculation. Then, the problem is truncated into a one-body system. By defining the center of mass M and the reduced mass μ as

$$M = m_1 + m_2, \qquad \mu = \frac{m_1 m_2}{m_1 + m_2} \tag{2}$$

with the center-of-mass and relative coordinates

$$\boldsymbol{R} = \frac{m_1\boldsymbol{r}_1 + m_2\boldsymbol{r}_2}{m_1 + m_2}, \qquad \boldsymbol{r} = \boldsymbol{r}_1 - \boldsymbol{r}_2, \tag{3}$$

respectively, the Hamiltonian can be split into the center-of-mass part H_R and relative motion part H_r as

$$H = H_R + H_r, \tag{4a}$$

$$H_R = -\frac{\hbar^2}{2M}\nabla_R^2, \tag{4b}$$

$$H_r = -\frac{\hbar^2}{2\mu}\nabla_r^2 + V^{\text{int}}(\boldsymbol{r}). \tag{4c}$$

The center-of-mass part H_R can be omitted because it describes the behavior of a free particle. Thus, only the relative motion part H_r is considered in this study.

For example, we assume that the interaction between particles depends only on the relative distance and is spherically symmetric. Then, the wave function can be expanded using spherical harmonics. The relative motion part of the Hamiltonian of the radial wave function reads

$$H_r = -\frac{\hbar^2}{2\mu}\left(\frac{\partial^2}{\partial r^2} + \frac{2}{r}\frac{\partial}{\partial r}\right) + \frac{\hbar^2 l(l+1)}{2\mu r^2} + V^{\text{int}}(r) \tag{5}$$

with l being the orbital quantum number. The ground-state energy of H_r is denoted as E_0.

2.2 Argonne series nucleon-nucleon potentials

Compared to the interaction between two electrons, nuclear interactions are much more complex, including isospin dependence and noncentral tensor force. In the following, we consider a Hamiltonian with the Argonne V18 (AV18) potential [61] to illustrate the present method [62–68]. [2] The AV18 potential is a nucleon–nucleon potential with explicit charge dependence and charge asymmetry, and it is composed of 18 operators

$$V^{\text{int}}(r) = \sum_{p=1}^{18} V_p(r) O^p. \tag{6}$$

The term O^p denotes a series of 18 operators. The first 14 operators are charge independent,

$$\begin{aligned} O^{p=1\text{–}14} &= \left[1,\ (\boldsymbol{\sigma}_1\cdot\boldsymbol{\sigma}_2),\ S_{12},\ (\boldsymbol{L}\cdot\boldsymbol{S}),\ \boldsymbol{L}^2,\ \boldsymbol{L}^2(\boldsymbol{\sigma}_1\cdot\boldsymbol{\sigma}_2),\ (\boldsymbol{L}\cdot\boldsymbol{S})^2\right] \\ &\quad \otimes \left[1,\ (\boldsymbol{\tau}_1\cdot\boldsymbol{\tau}_2)\right], \end{aligned} \tag{7}$$

and the last four break the charge independence,

$$O^{p=15\text{–}18} = \left[1,\ (\boldsymbol{\sigma}_1\cdot\boldsymbol{\sigma}_2),\ S_{12}\right] \otimes T_{12},\ (\tau_{z1} + \tau_{z2}). \tag{8}$$

The operators include the Pauli matrices of spin $\boldsymbol{\sigma}$ and isospin $\boldsymbol{\tau}$, the z-projection of isospin τ_z, the product of orbital angular momentum $\boldsymbol{L}$ and spin $\boldsymbol{S}$, and the tensor operator S_{12} and the isotensor operator T_{12} defined by

$$S_{12} = 3\frac{(\boldsymbol{\sigma}_1\cdot\boldsymbol{r})(\boldsymbol{\sigma}_2\cdot\boldsymbol{r})}{r^2} - \boldsymbol{\sigma}_1\cdot\boldsymbol{\sigma}_2, \tag{9a}$$

$$T_{12} = 3\tau_{z1}\tau_{z2} - \boldsymbol{\tau}_1\cdot\boldsymbol{\tau}_2, \tag{9b}$$

respectively. The $V_p(r)$ are obtained by fitting into the two-nucleon scattering data and the deuteron binding energy [61]. On top of the nuclear interaction defined by Eq. (6) and the proton-proton Coulomb interaction, the higher-order corrections of the electromagnetic interactions are included. Hence, an electromagnetic interaction exists between a proton and a neutron.

Besides the AV18 potential, for the calculation of the deuteron we will also use the Argonne V8′ (AV8′) [69] and the Argonne V4′ (AV4′) [70] potentials. The AV8′ potential is a simplified version of the AV18 potential with the number of operators reducing from 18 to 8,

[2] It should be noted that any local potentials, including the state-of-the-arts chiral effective potentials [62–68], can be used in our method, while this method can also be applied for the momentum-space representation straightforwardly.

$$O^{p=1-8} = \left[1,\ (\boldsymbol{\sigma}_1 \cdot \boldsymbol{\sigma}_2),\ S_{12},\ (\boldsymbol{L} \cdot \boldsymbol{S})\right] \otimes \left[1,\ (\boldsymbol{\tau}_1 \cdot \boldsymbol{\tau}_2)\right]. \tag{10}$$

The AV4′ potential is a further simplified version with the number of operators reducing from 8 to 4,

$$O^{p=1-4} = \left[1,\ (\boldsymbol{\sigma}_1 \cdot \boldsymbol{\sigma}_2)\right] \otimes \left[1,\ (\boldsymbol{\tau}_1 \cdot \boldsymbol{\tau}_2)\right]. \tag{11}$$

The radial potentials $V_p(r)$ for both AV8′ and AV4′ potentials are a linear combination of $V_p(r)$ of the AV18 potential.

2.3 Partial wave expansion of wave function

To find the ground state of the selected Hamiltonian, we rewrite the quantum state using the partial wave expansion

$$|\Psi\rangle = \sum_{\substack{L, m_L, S,\\ m_S, T, m_T}} a_{Lm_L Sm_S Tm_T} \varphi_{Lm_L Sm_S Tm_T} Y_{Lm_L} |Sm_S\rangle \otimes |Tm_T\rangle. \tag{12}$$

The $\varphi_{Lm_L Sm_S Tm_T}$ denotes the radial part of the wave function. The Y_{Lm_L}, $|Sm_S\rangle$, and $|Tm_T\rangle$ are the eigenstates of operators $\boldsymbol{L}$, $\boldsymbol{S}$, and $\boldsymbol{T}$, respectively. Because the deuteron is an isospin singlet state ($T = 0$), we only consider $|Tm_T\rangle = |00\rangle$ and omit it in the following. We assume partial wave functions are normalized, i.e.,

$$\sum_{\substack{L, m_L,\\ S, m_S}} a^2_{Lm_L Sm_S} = 1. \tag{13}$$

Because there exists the $(\boldsymbol{L} \cdot \boldsymbol{S})$ term in the AV18 and AV8′ potentials, the quantum numbers $L(L+1)$ and $S(S+1)$ are no longer good quantum numbers. Therefore, we introduce $J(J+1)$ as a good quantum number, which is the eigenvalue of the squared total angular momentum operator $\boldsymbol{J}^2$, where $\boldsymbol{J} = \boldsymbol{L} + \boldsymbol{S}$. By changing the basis of partial waves, the new expansion of the wave function reads

$$\begin{aligned} |\Psi\rangle &= \sum_{\substack{L, m_L,\\ S, m_S}} a_{Lm_L Sm_S} \varphi_{Lm_L Sm_S} Y_{Lm_L} |Sm_S\rangle \\ &= \sum_{\substack{L, S,\\ J, m_J}} b_{LSJm_J} \psi_{LSJm_J} |LSJm_J\rangle \end{aligned} \tag{14}$$

with the normalization condition for the new coefficients

$$\sum_{\substack{L, S,\\ J, m_J}} b^2_{LSJm_J} = 1. \tag{15}$$

By utilizing the Clebsch-Gordan coefficients $c^{Jm_J}_{j_1 m_{j_1} j_2 m_{j_2}}$, we have the expansion

$$|LSJm_J\rangle = \sum_{m_L, m_S} c^{Jm_J}_{Lm_L Sm_S} Y_{Lm_L} |Sm_S\rangle. \tag{16}$$

Therefore, the wave function can be simplified as

$$|\Psi\rangle = \sum_{\substack{L, S,\\ J, m_J}} b_{LSJm_J} \psi_{LSJm_J} \sum_{m_L, m_S} c^{Jm_J}_{Lm_L Sm_S} Y_{Lm_L} |Sm_S\rangle. \tag{17}$$

Because of the $SO(3)$ symmetry for J, the states with different m_J degenerate

$$d_{LSJ} \phi_{LSJ} = b_{LSJm_J} \psi_{LSJm_J}. \tag{18}$$

The final partial wave expansion is

$$|\Psi\rangle = \sum_{L,S,J} d_{LSJ} \phi_{LSJ} \sum_{m_L, m_S, m_J} c^{Jm_J}_{Lm_L Sm_S} Y_{L,m_L} |Sm_S\rangle \tag{19}$$

with the normalization condition

$$\sum_{L,S,J} d^2_{LSJ} (2J+1) = 1. \tag{20}$$

3 Neural network models

3.1 The discrete form of Hamiltonian and wave functions in a neural network

In the present neural network approach, the wave function is represented using a DNN. Because we focus only on the bound states of systems, it is sufficient to calculate the system within a box of finite size. The spatial coordinate r is discretized as the input variables and the partial wave functions ϕ_{LSJ} are the output variables of the DNN, so that they can be represented as vectors. The function $\xi_{LSJ}(r) = r\phi_{LSJ}(r)$ is defined to impose the Dirichlet boundary condition $\xi_{LSJ}(0) = \xi_{LSJ}(\infty) = 0$ for the loss function calculation. The function ξ_{LSJ} satisfies

$$H'_r \xi_{LSJ}(r) = E_0 \xi_{LSJ}(r), \tag{21}$$

where H'_r reads

$$H'_r = -\frac{\hbar^2}{2\mu} \frac{\partial^2}{\partial r^2} + \frac{\hbar^2 l(l+1)}{2\mu r^2} + V^{\text{int}}(r). \tag{22}$$

To perform the calculation numerically, the mesh points of the spatial coordinates are evenly distributed with size Δr, with $(M+1)$ mesh points in total. Because the boundary condition is assumed as $\xi(0) = \xi(r_{\text{Max}}) = 0$, only $(M-1)$ mesh points are calculated. In detail, the output of the DNN

is used as ϕ_{LSJ}, and the loss function is calculated by using ξ_{LSJ}, since using ϕ_{LSJ} as the output provides better accuracy than using ξ_{LSJ} as shown in the Appendix. The $\phi(0)$ is calculated using the Lagrange interpolating polynomial with five adjacent points. The vector corresponding to the radial partial wave function ϕ_{LSJ} of Eq. (19) reads

$$\phi_{LSJ} \simeq \begin{pmatrix} \tilde{\phi}_{LSJ1} \\ \tilde{\phi}_{LSJ2} \\ \tilde{\phi}_{LSJ3} \\ \vdots \\ \tilde{\phi}_{LSJ(M-3)} \\ \tilde{\phi}_{LSJ(M-2)} \\ \tilde{\phi}_{LSJ(M-1)} \end{pmatrix}, \tag{23}$$

where the i-th component is

$$\tilde{\phi}_{LSJ_i} = \phi_{LSJ}(r_i), \tag{24}$$

with $r_i = i\,\Delta r$.

The second derivative in the H'_r reads

$$\frac{\partial^2}{\partial r^2} \simeq \frac{1}{(\Delta r)^2} \begin{pmatrix} -2 & 1 & 0 & \dots & 0 & 0 & 0 \\ 1 & -2 & 1 & \dots & 0 & 0 & 0 \\ 0 & 1 & -2 & \dots & 0 & 0 & 0 \\ \vdots & \vdots & \vdots & \ddots & \vdots & \vdots & \vdots \\ 0 & 0 & 0 & \dots & -2 & 1 & 0 \\ 0 & 0 & 0 & \dots & 1 & -2 & 1 \\ 0 & 0 & 0 & \dots & 0 & 1 & -2 \end{pmatrix}. \tag{25}$$

The rest part of H'_r, denoted as V altogether, are expressed as diagonal matrices

$$V \simeq \begin{pmatrix} \tilde{V}_1 & 0 & 0 & \dots & 0 & 0 & 0 \\ 0 & \tilde{V}_2 & 0 & \dots & 0 & 0 & 0 \\ 0 & 0 & \tilde{V}_3 & \dots & 0 & 0 & 0 \\ \vdots & \vdots & \vdots & \ddots & \vdots & \vdots & \vdots \\ 0 & 0 & 0 & \dots & \tilde{V}_{M-3} & 0 & 0 \\ 0 & 0 & 0 & \dots & 0 & \tilde{V}_{M-2} & 0 \\ 0 & 0 & 0 & \dots & 0 & 0 & \tilde{V}_{M-1} \end{pmatrix}, \tag{26}$$

where $\tilde{V}_i = V(r_i)$. The ground-state energy E_0 can then be calculated by

$$E_0 \simeq \frac{\langle \Psi | H | \Psi \rangle}{\langle \Psi | \Psi \rangle}. \tag{27}$$

3.2 The design of the non-fully connected neural network

The design of the present non-fully connected DNN, which generates partial wave functions with corresponding coefficients $d_j\phi_j$, is shown in Fig. 1. The input is the relative distance r_i. The outputs are the partial wave functions. After determining the cutoff value of the orbital angular momentum L and the spin quantum number S, the possible angular momentum sets $\{LSJ\}$ of partial waves are then determined by the LS coupling. For each single output, the nodes in the hidden layers are fully connected, while the hidden layer nodes of different outputs are not connected to each other. The "softplus" function

$$\text{softplus}\,(x) = \log\,(1 + e^x) \tag{28}$$

is used as the activation function.

Throughout the training process, the relative distances of the particles are discretized into M uniformly distributed lattice points, which are passed to the DNN as a dataset. The output of the DNN is a dataset containing all partial wave

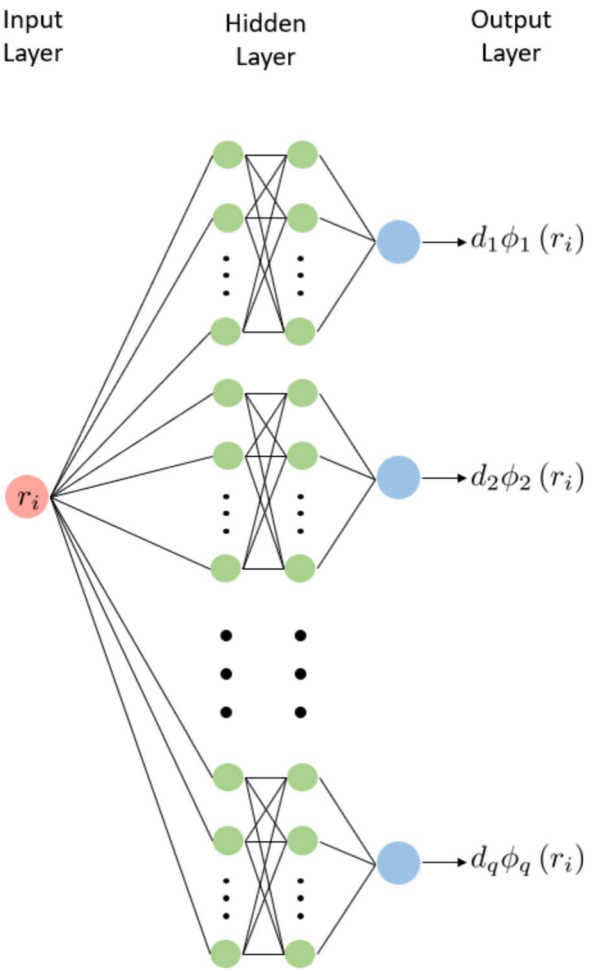

Fig. 1 Schematic figure of a non-fully connected deep neural network. The shared input is the relative distance between the particles. The outputs are the partial wave functions with coefficients $d_j\phi_j$, where j ($j = 1, 2, ..., q$) represents the combination of the angular momenta, L, S, and J. There is no connection between the hidden layer nodes of different outputs. The computational accuracy can be enhanced by increasing the number of layers and nodes in each layer

functions. The energy expectation value is regarded as the loss function, which is calculated using Eq. (27). The parameters of DNN are then updated by the Adam optimizer [71] and the ML is implemented by using the TENSORFLOW [72].

4 Calculation results for deuteron

The feasibility of the method was validated by applying it to deuterons. To include a more general case, at the beginning, we consider the orbital angular momentum quantum number L from zero to four and spin quantum number S from zero to one in Eq. (24) with 18 possible states. The 18 partial wave functions are computed in a 20 fm box with 1500 mesh points. A non-fully connected DNN is used, which is composed of two layers, each containing 16 units. Moreover, we also tested a fully connected version of such a DNN to explore the impact of connections between nodes on the training results. Both models are trained to testify whether only the $^3S_1$ and $^3D_1$ states are obtained, which is a known fact regarding the properties of deuterons [73]. Table 1 lists the percentage of each state in the wave function. The results show that only the $^3S_1$ and $^3D_1$ states make significant contributions in the ground state, while the contributions of the other states are sufficiently small to be neglected, which is consistent with the known fact. It was also found that both the fully connected and non-fully connected DNN can generate the ground state with the same level of accuracy, showing that the connection between nodes does not make a significant difference in precision. We chose the non-fully connected one for subsequent calculations. The relative error of the ground-state energy is 0.05 % of the benchmark value obtained by the Green's function Monte Carlo calculation [61].

Since it is proved that only the $^3S_1$ and $^3D_1$ states contribute to the ground-state energy, we can reduce the number of outputs from 18 to 2 to reduce the size of the DNN. Accordingly, the calculation cost is also reduced; hence, hereinafter we apply a more complicated hidden layer structure that is composed of three layers each containing 16 units with 30 fm box size and 2000 mesh points. The energies obtained using the AV18, AV8′, and AV4′ potentials are listed in Table 2. In order to see the effect of the electromagnetic interaction between a proton and a neutron, calculations using the AV8′ potential with and without the electromagnetic interaction are also shown. The accuracy is both within 2 keV (0.1 %) for AV18 and AV8′ calculations compared to the benchmark

Table 2 DNN results for the energies of the deuteron in the AV18, AV8′ (with and without the electromagnetic (EM) interaction), and AV4′ potentials

	Energy (MeV)	Relative error
Benchmark (AV18) [61]	−2.2246	
AV18 (with EM)	−2.2258	0.054 %
AV8′ (with EM)	−2.2259	0.058 %
AV8′ (without EM)	−2.2434	0.845 %
AV4′ (without EM)	−2.2436	0.854 %

There exist about 1 % relative errors in the AV8′ (without the EM) and AV4′ results [70]. The hidden layers of each output are composed of three layers, each of which has 16 units. The benchmark energy is taken from Ref. [61]

Table 1 Percentage of 18 partial wave states to the wave function with the AV18 potential

		Non-fully connected		Fully connected	
		$S=1$	$S=0$	$S=1$	$S=0$
$L=0$	$J=0$		7.4428×10^{-9}		5.3286×10^{-9}
	$J=1$	0.9423		0.9422	
	$J=0$	8.5079×10^{-11}		8.3838×10^{-10}	
$L=1$	$J=1$	9.3388×10^{-8}	3.5507×10^{-11}	8.8066×10^{-10}	9.1213×10^{-9}
	$J=2$	2.6372×10^{-9}		2.6894×10^{-7}	
	$J=1$	0.0577		0.0578	
$L=2$	$J=2$	4.3943×10^{-11}	4.6278×10^{-12}	7.2171×10^{-8}	1.1914×10^{-8}
	$J=3$	3.2904×10^{-8}		9.3754×10^{-9}	
	$J=2$	1.4599×10^{-9}		4.0260×10^{-9}	
$L=3$	$J=3$	1.0769×10^{-11}	4.8327×10^{-9}	9.0229×10^{-9}	3.1785×10^{-9}
	$J=4$	1.4207×10^{-9}		8.0821×10^{-9}	
	$J=3$	2.3481×10^{-9}		4.2018×10^{-9}	
$L=4$	$J=4$	1.8652×10^{-9}	5.2457×10^{-9}	4.8368×10^{-9}	4.8066×10^{-9}
	$J=5$	6.4078×10^{-9}		1.0747×10^{-7}	

The ground-state energy reads −2.2241 MeV and −2.2246 MeV for the non-fully and fully connected neural networks, with both within 0.03 % relative error with respect to the benchmark value [61]. Each unconnected hidden layers are two layers, each of which is composed of 16 units

[61]. The AV4′ potential comprises only four terms; hence, it yields a final error of approximately 1 % [70]. In Fig. 2, the deuteron wave functions are shown based on AV18 and AV8′ potentials, which are compared with deuteron wave functions of the AV18 calculation in Ref. [61]. It is observed that the DNN results of both AV18 and AV8′ calculations reproduce the AV18 benchmark [61] quite nicely. The relative errors $\left[u^{\mathrm{DNN}}(r) - u^{\mathrm{benchmark}}(r)\right]/u^{\mathrm{benchmark}}(r)$ and $\left[w^{\mathrm{DNN}}(r) - w^{\mathrm{benchmark}}(r)\right]/w^{\mathrm{benchmark}}(r)$ are shown in Fig. 3, where u and w are the partial wave functions of $^3S_1$ and $^3D_1$ states, respectively. Because the contribution of the $^3D_1$ state in the loss function is much smaller than that of $^3S_1$, its relative error is accordingly larger.

The DNN energies with respect to different numbers of mesh points in the AV18 potential are listed in Table 3. It was found that 500 mesh points were sufficiently large to produce results with less than 1 % relative error, with the fluctuation of the DNN training results becoming an important factor in the precision.

Table 4 shows the performance of the program by varying the number of layers and nodes with the AV18 potential [74–76]. In the case of a single hidden layer containing 16 units, the relative error in energy is 2.857 %. With an increase in the number of units to 32 or the addition of a hidden layer, the relative errors do not exceed 0.1 %. A more complicated network structure does not result in higher precision, as the training results fluctuate slightly every time.

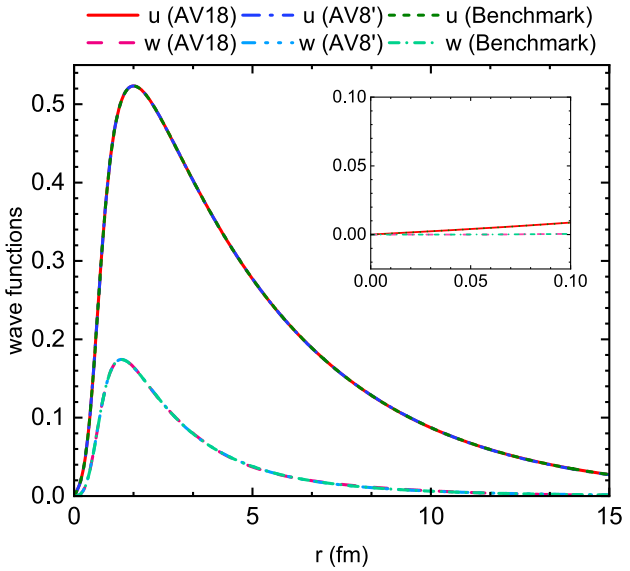

Fig. 2 Deuteron wave functions with the AV18 and AV8′ potentials, where u and w denote the S-wave and D-wave components, respectively. The benchmark is based on the AV18 potential [61] taken from Ref. [74]. The hidden layers of each output are composed of three layers, each of which has 16 units. Both results of the AV18 and AV8′ potentials show good agreement with the benchmark

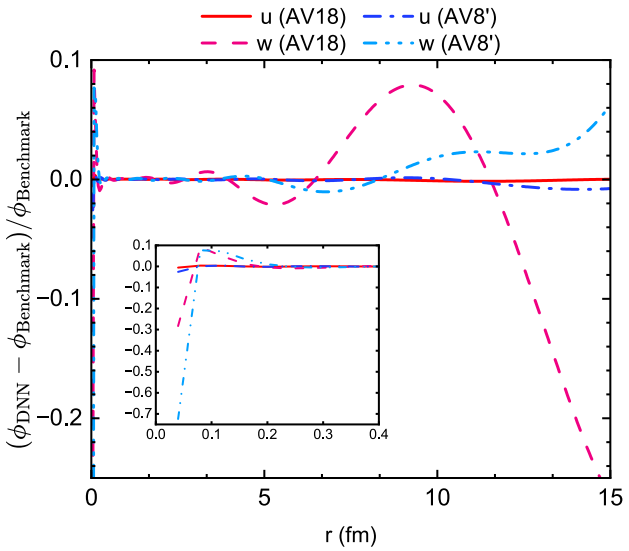

Fig. 3 Relative error of DNN deuteron wave functions to the AV18 benchmark results [61, 74]. The hidden layers of each output are composed of three layers each of which has 16 units

This finding differs from that of Ref. [42], where adding a second layer induces a sharp decrease in model accuracy, whereas increasing the number of hidden nodes partially compensates for this loss. This shows that our DNN model is more stable and can be effectively extended to model complex physical systems, where expressive power necessitates the use of deeper network architectures.

In Fig. 4, the relative errors of the loss function with respect to the benchmark energy are shown as functions of epochs in the AV18 calculation for two optimizers. When the Adam optimizer was used, spikes appeared in the loss values, although the loss still decreased between them. In contrast, when we use the stochastic gradient descent (SGD) optimizer [77], these spikes do not appear; instead, it requires more steps to reach convergence.

Table 3 DNN energies with respect to different numbers of mesh points in the AV18 potential

Number of mesh points	Energy (MeV)	Relative error (%)
200	−2.3659	2.729
500	−2.2248	0.008
1000	−2.2297	0.229
1500	−2.2265	0.085
2000	−2.2258	0.054
Benchmark (AV18) [61]	−2.2246	

500 mesh points are sufficient to generate results within 1 % relative error, while the relative error barely reduces as the mesh points increase from 1200 to 1500

Table 4 Performance test of deuteron calculation in the AV18 potential

# of unit in layers			Energy	Relative error (%)	D state prob. (%)
1st	2nd	3rd	(MeV)		
16	–	–	−2.16215	2.857	5.70
32	–	–	−2.22552	0.042	5.77
16	16	–	−2.22536	0.035	5.77
16	32	–	−2.22588	0.058	5.77
32	16	–	−2.22569	0.049	5.77
32	32	–	−2.22580	0.055 %	5.77
16	16	16	−2.22581	0.055	5.77
32	32	32	−2.22575	0.053	5.77
Expt. [75, 76]			−2.22458		
Benchmark (AV18) [61]			−2.22458		5.76

Rows with "–" in the column "# of unit in layers" represent an empty layer. The benchmark values with the AV18 [61] and the experimental data [75, 76] are listed in the last row

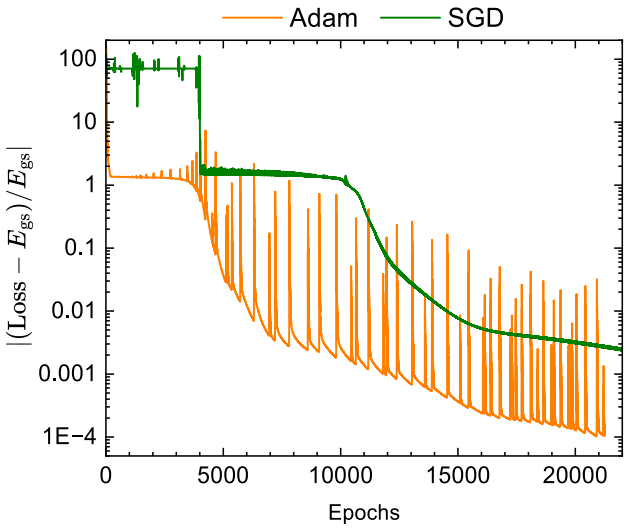

Fig. 4 Relative error of $\langle H \rangle$ with respect to the benchmark AV18 ground-state energy $E_{\text{gs}} = -2.22458$ MeV [75, 76] as functions of the number of epochs. The hidden layers of each output were composed of three layers, each of which has 16 units. The DNN with the Adam optimizer converges around 20000 epochs, while the one with the SGD optimizer fails to converge within 10^5 epochs

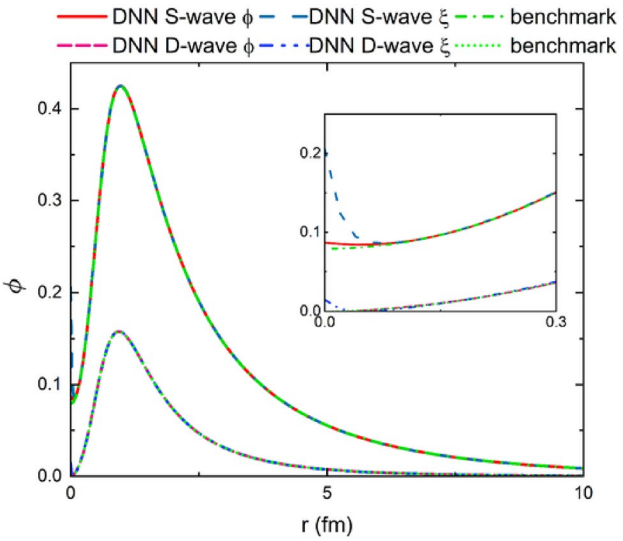

Fig. 5 Wave functions ϕ_{LSJ} obtained by 1) the output corresponds to ξ_{LSJ} (Blue) and 2) the output corresponding to ϕ_{LSJ} and ξ_{LSJ} is calculated from the output (Red). The benchmark calculation [61] is also shown (Green)

5 Summary

In Ref. [57], an unsupervised machine learning technique was developed to calculate the ground state using a deep neural network. In this study, we extended the method by introducing spin and isospin degrees of freedom through the introduction of partial wave expansions generated by a non-fully connected deep neural network.

The method was verified by calculating the simplest two-body nuclear system—deuteron. At first, the partial waves with the orbital angular momentum quantum number L from zero to four and the possible total spin S from zero to one were calculated. The results were consistent with the fact that only the $^3S_1$ and $^3D_1$ states contribute to the deuteron ground state. In the following calculations, the obtained wave functions and energies showed consistency with the benchmark [61, 70]. We found that the deep neural network does not need to be large. In the present case, two hidden layers, each containing eight units, were sufficient to generate faithful representations of the wave function.

We believe that these improvements to the deep neural network approach hold promise for further studies that could extend the methodology of this work. For example, one can extend from two-body calculations to N-body calculations.

For three-body systems, we believe the ground state can be obtained by solving the Faddeev equation using hyperspherical coordinates [78], in which the corresponding partial wave expansion includes two angular terms with spin and isospin components. Based on the present work and our deep neural network approach to solve the Dirac equation [79], another promising direction is to incorporate the spin and isospin degrees of freedom into the Dirac framework. We anticipate that the present deep neural network architecture can be extended to generate Dirac partial wave functions.

DNN output analysis

We show the wave functions corresponding to the two strategies for selecting the DNN outputs: (1) the output corresponds to ξ_{LSJ} and (2) the output corresponding to ϕ_{LSJ} and ξ_{LSJ} is calculated from the output, as did in the main text. In our test, we use 1700 mesh points in a 20 fm box to generate $^3S_1$ and $^3D_1$ states. We find that the DNN can generate more precise results of ϕ_{LSJ} than ξ_{LSJ} close to the origin, as shown in Fig. 5. Therefore, ϕ_{LSJ} was utilized as the DNN output in our calculation.

Acknowledgements The authors thank Koji Hashimoto and Hisashi Naito for fruitful discussions. C.W. acknowledges the warm hospitality of the RIKEN iTHEMS Center.

Author Contributions All authors contributed to the study conception and design. Conceptualization was done by Tomoya Naito, Jian Li, and Haozhao Liang. Methodology was proposed by all the authors. Calculation and the data analysis were performed by Chuanxin Wang. The supervision was by Tomoya Naito, Jian Li, and Haozhao Liang. The first draft of the manuscript was written by Chuanxin Wang and Tomoya Naito; all the authors commented on the manuscript. All the authors read and approved the final manuscript.

Funding Open Access funding provided by The University of Tokyo.

Declarations

Conflict of interest The authors declare that they have no conflict of interest.

References

1. P. Hohenberg, W. Kohn, Inhomogeneous electron gas. Phys. Rev. **136**, B864 (1964). https://doi.org/10.1103/PhysRev.136.B864
2. W. Kohn, L.J. Sham, Self-consistent equations including exchange and correlation effects. Phys. Rev. **140**, A1133 (1965). https://doi.org/10.1103/PhysRev.140.A1133
3. W. Kohn, Nobel lecture: electronic structure of matter–wave functions and density functionals. Rev. Mod. Phys. **71**, 1253 (1999). https://doi.org/10.1103/RevModPhys.71.1253
4. S.R. White, Density matrix formulation for quantum renormalization groups. Phys. Rev. Lett. **69**, 2863 (1992). https://doi.org/10.1103/PhysRevLett.69.2863
5. H. Shinaoka, D. Geffroy, M. Wallerberger et al., Sparse sampling and tensor network representation of two-particle Green's functions. SciPost Phys. **8**, 012 (2020). https://doi.org/10.21468/SciPostPhys.8.1.012
6. W.L. McMillan, Ground state of liquid He ^{4}. Phys. Rev. **138**, A442 (1965). https://doi.org/10.1103/PhysRev.138.A442
7. D. Ceperley, G.V. Chester, M.H. Kalos, Monte Carlo simulation of a many-fermion study. Phys. Rev. B **16**, 3081 (1977). https://doi.org/10.1103/PhysRevB.16.3081
8. D.M. Ceperley, B.J. Alder, Ground state of the electron gas by a stochastic method. Phys. Rev. Lett. **45**, 566 (1980). https://doi.org/10.1103/PhysRevLett.45.566
9. G. Carleo, M. Troyer, Solving the quantum many-body problem with artificial neural networks. Science **355**, 602 (2017). https://doi.org/10.1126/science.aag2302
10. Y. Nomura, A.S. Darmawan, Y. Yamaji et al., Restricted Boltzmann machine learning for solving strongly correlated quantum systems. Phys. Rev. B **96**, 205152 (2017). https://doi.org/10.1103/PhysRevB.96.205152
11. G. Carleo, Y. Nomura, M. Imada, Constructing exact representations of quantum many-body systems with deep neural networks. Nat. Commun. **9**, 5322 (2018). https://doi.org/10.1038/s41467-018-07520-3
12. J. Stokes, J.R. Moreno, E.A. Pnevmatikakis et al., Phases of two-dimensional spinless lattice fermions with first-quantized deep neural-network quantum states. Phys. Rev. B **102**, 205122 (2020). https://doi.org/10.1103/PhysRevB.102.205122
13. K. Choo, G. Carleo, N. Regnault et al., Symmetries and many-body excitations with neural-network quantum states. Phys. Rev. Lett. **121**, 167204 (2018). https://doi.org/10.1103/PhysRevLett.121.167204
14. Y. Nomura, Machine learning quantum states – extensions to Fermion-boson coupled systems and excited-state calculations. J. Phys. Soc. Jpn. **89**, 054706 (2020). https://doi.org/10.7566/JPSJ.89.054706
15. A. Boehnlein, M. Diefenthaler, N. Sato et al., Colloquium: machine learning in nuclear physics. Rev. Mod. Phys. **94**, 031003 (2022). https://doi.org/10.1103/RevModPhys.94.031003
16. W. He, Q. Li, Y. Ma et al., Machine learning in nuclear physics at low and intermediate energies. Sci. China Phys. Mech. Astron. **66**, 282001 (2023). https://doi.org/10.1007/s11433-023-2116-0
17. Y. Lu, T. Shang, P. Du, J. Li, H. Liang, Z. Niu. Nuclear mass predictions based on a convolutional neural network. Phys. Rev. C **111**(1), 014325 (2025). https://doi.org/10.1103/PhysRevC.111.014325
18. Z.M. Niu, H.Z. Liang. Nuclear mass predictions with machine learning reaching the accuracy required by r-process studies. Phys. Rev. C **106**(2), L021303 (2022). https://doi.org/10.1103/PhysRevC.106.L021303
19. Gao ZP, Wang YJ, Lü HL, Li QF, Shen CW, Liu L. Machine learning the nuclear mass. Nucl. Sci. Tech. **32**(10):109 (2021). https://doi.org/10.1007/s41365-021-00956-1

20. Z.Y. Yuan, D. Bai, Z. Wang, Z.Z. Ren. Reliable calculations of nuclear binding energies by the Gaussian process of machine learning. Nucl. Sci. Tech. **35**(6), 105 (2024). https://doi.org/10.1007/s41365-024-01463-9
21. X.C. Ming, H.F. Zhang, R.R. Xu, X.D. Sun, Y. Tian, Z.G. Ge. Nuclear mass based on the multi-task learning neural network method. Nucl. Sci. Tech. **33**(4), 48 (2022). https://doi.org/10.1007/s41365-022-01031-z
22. Y.-Y. Cao, J.-Y. Guo, B. Zhou, Predictions of nuclear charge radii based on the convolutional neural network. Nucl. Sci. Tech. **34**, 152 (2023). https://doi.org/10.1007/s41365-023-01308-x
23. L. Tang, Z.-H. Zhang, Nuclear charge radius predictions by kernel ridge regression with odd-even effects, Nucl. Sci. Tech. **35**, 19 (2024). https://doi.org/10.1007/s41365-024-01379-4
24. H. Liu, X.-X. Li, Y. Yuan et al., Prediction of the first 2^+ states properties for atomic nuclei using light gradient boosting machine. Nucl. Sci. Tech. **36**, 21 (2025). https://doi.org/10.1007/s41365-024-01613-z
25. J.H. Bai, Z.M. Niu, B.Y. Sun et al., The description of giant dipole resonance key parameters with multitask neural networks. Phys. Lett. B **815**, 136147 (2021). https://doi.org/10.1016/j.physletb.2021.136147
26. U. Baños Rodríguez, C. Zuñiga Vargas, M. Gonçalves et al., Alpha half-lives calculation of superheavy nuclei with Qα-value predictions based on the Bayesian neural network approach. J. Phys. G **46**, 115109 (2019). https://doi.org/10.1088/1361-6471/ab2c86
27. U. Baños Rodríguez, C. Zuñiga Vargas, M. Gonçalves et al., Bayesian neural network improvements to nuclear mass formulae and predictions in the SuperHeavy Elements region. Europhys. Lett. **127**, 42001 (2019). https://doi.org/10.1209/0295-5075/127/42001
28. Z.M. Niu, H.Z. Liang, B.H. Sun et al., Predictions of nuclear β-decay half-lives with machine learning and their impact on r-process nucleosynthesis. Phys. Rev. C **99**, 064307 (2019). https://doi.org/10.1103/PhysRevC.99.064307
29. P. Li, Z.-M. Niu, Y.-F. Niu, Selection of abnormal trends in nuclear β-decay half-lives by neural network and exploration of the physical mechanisms. Nucl. Sci. Tech. **36**, 50 (2025). https://doi.org/10.1007/s41365-025-01663-x
30. T.-S. Shang, J. Li, Z.-M. Niu, Prediction of nuclear charge density distribution with feedback neural network. Nucl. Sci. Tech. **33**, 153 (2022). https://doi.org/10.1007/s41365-022-01140-9
31. T.S. Shang, H.H. Xie, J. Li et al., Global prediction of nuclear charge density distributions using a deep neural network. Phys. Rev. C **110**, 014308 (2024). https://doi.org/10.1103/PhysRevC.110.014308
32. W. Yundong, T. Shang, D.H. Xie, M.P. Du, D.J. Li, H. Liang. China Xiv:202510.00163 (2025)
33. Z.-X. Yang, X.-H. Fan, Z.-P. Li et al., A Kohn-Sham scheme based neural network for nuclear systems. Phys. Lett. B **840**, 137870 (2023). https://doi.org/10.1016/j.physletb.2023.137870
34. P.-X. Du, T.-S. Shang, K.-P. Geng et al., Inference of parameters for the back-shifted Fermi gas model using a feedforward neural network. Phys. Rev. C **109**, 044325 (2024). https://doi.org/10.1103/PhysRevC.109.044325
35. X. Wang, Y. Cui, Y. Tian, K. Zhao, Y. Zhang. Uncertainties of nuclear level density estimated using Bayesian neural networks. Chin. Phys. C **48**(8), 084105 (2024). https://doi.org/10.1088/1674-1137/ad47a7
36. Z. Yuan, D. Tian, J. Li et al., Magnetic moment predictions of odd-A nuclei with the Bayesian neural network approach. Chin. Phys. C **45**, 124107 (2021). https://doi.org/10.1088/1674-1137/ac28f9
37. E. Parnes, N. Barnea, G. Carleo et al., Nuclear responses with neural-network quantum states (2025), arXiv:2504.20195 [nucl-th]
38. Z.-X. Zhang, Y.-L. Yang, W.-B. He et al., Machine learning the single-Λ hypernuclei with neural-network quantum states (2025), arXiv:2508.03575 [nucl-th]
39. D. Liu, A. Noor A, Z.-Z. Qin et al., Neural network study of the nuclear ground-state spin distribution within a random interaction ensemble. Nucl. Sci. Tech. **35**, 64 (2024). https://doi.org/10.1007/s41365-024-01424-2
40. H. Yoshino, Spatially heterogeneous learning by a deep student machine. Phys. Rev. Res. **5**, 033068 (2023). https://doi.org/10.1103/PhysRevResearch.5.033068
41. J.W.T. Keeble, A. Rios, Machine learning the deuteron. Phys. Lett. B **809**, 135743 (2020). https://doi.org/10.1016/j.physletb.2020.135743
42. J. Rozalén Sarmiento, J.W.T. Keeble, A. Rios, Machine learning the deuteron: new architectures and uncertainty quantification. Eur. Phys. J. Plus **139**, 189 (2024). https://doi.org/10.1140/epjp/s13360-024-04983-w
43. H. Saito, Method to solve quantum few-body problems with artificial neural networks. J. Phys. Soc. Jpn. **87**, 074002 (2018). https://doi.org/10.7566/JPSJ.87.074002
44. G. Pescia, J. Han, A. Lovato et al., Neural-network quantum states for periodic systems in continuous space. Phys. Rev. Res. **4**, 023138 (2022). https://doi.org/10.1103/PhysRevResearch.4.023138
45. D. Pfau, J.S. Spencer, A.G.D.G. Matthews et al., Ab initio solution of the many-electron Schrödinger equation with deep neural networks. Phys. Rev. Res. **2**, 033429 (2020). https://doi.org/10.1103/PhysRevResearch.2.033429
46. J. Hermann, Z. Schätzle, F. Noé, Deep-neural-network solution of the electronic Schrödinger equation. Nat. Chem. **12**, 891 (2020). https://doi.org/10.1038/s41557-020-0544-yhttps://www.nature.com/articles/s41557-020-0544-y
47. C. Adams, G. Carleo, A. Lovato et al., Variational Monte Carlo calculations of $A \leq 4$ nuclei with an artificial neural-network correlator Ansatz. Phys. Rev. Lett. **127**, 022502 (2021). https://doi.org/10.1103/PhysRevLett.127.022502
48. A. Gnech, C. Adams, N. Brawand et al., Nuclei with Up to $A = 6$ nucleons with artificial neural network wave functions. Few-Body Syst. **63**, 7 (2022). https://doi.org/10.1007/s00601-021-01706-0
49. Y.L. Yang, P.W. Zhao, A consistent description of the relativistic effects and three-body interactions in atomic nuclei. Phys. Lett. B **835**, 137587 (2022). https://doi.org/10.1016/j.physletb.2022.137587
50. Y.L. Yang, P.W. Zhao, Deep-neural-network approach to solving the ab initio nuclear structure problem. Phys. Rev. C **107**, 034320 (2023). https://doi.org/10.1103/PhysRevC.107.034320
51. B. Fore, J.M. Kim, G. Carleo et al., Dilute neutron star matter from neural-network quantum states. Phys. Rev. Res. **5**, 033062 (2023). https://doi.org/10.1103/PhysRevResearch.5.033062
52. J.R. Moreno, G. Carleo, A. Georges et al., Fermionic wave functions from neural-network constrained hidden states. Proc. Natl. Acad. Sci. U.S.A. **119**, e2122059119 (2022). https://doi.org/10.1073/pnas.2122059119
53. A. Lovato, C. Adams, G. Carleo et al., Hidden-nucleons neural-network quantum states for the nuclear many-body problem. Phys. Rev. Res. **4**, 043178 (2022). https://doi.org/10.1103/PhysRevResearch.4.043178
54. A. Gnech, B. Fore, A.J. Tropiano et al., Distilling the essential elements of nuclear binding via neural-network quantum states. Phys. Rev. Lett. **133**, 142501 (2024). https://doi.org/10.1103/PhysRevLett.133.142501
55. K. Choo, A. Mezzacapo, G. Carleo, Fermionic neural-network states for ab-initio electronic structure. Nat. Commun. **11**, 2368 (2020). https://doi.org/10.1038/s41467-020-15724-9

56. J. Hermann, J. Spencer, K. Choo et al., Ab initio quantum chemistry with neural-network wavefunctions. Nat. Rev. Chem. **7**, 692 (2023). https://doi.org/10.1038/s41570-023-00516-8
57. T. Naito, H. Naito, K. Hashimoto, Multi-body wave function of ground and low-lying excited states using unornamented deep neural networks. Phys. Rev. Res. **5**, 033189 (2023). https://doi.org/10.1103/PhysRevResearch.5.033189
58. K. Hornik, M. Stinchcombe, H. White, Multilayer feedforward networks are universal approximators. Neural Netw. **2**, 359 (1989). https://doi.org/10.1016/0893-6080(89)90020-8
59. K. Hornik, Approximation capabilities of multilayer feedforward networks. Neural Netw. **4**, 251 (1991). https://doi.org/10.1016/0893-6080(91)90009-T
60. J. W. Keeble, Neural network solutions to the fermionic Schrödinger equation type. PhD Thesis, school University of Surrey (2022). https://doi.org/10.15126/thesis.900505.
61. R.B. Wiringa, V.G.J. Stoks, R. Schiavilla, Accurate nucleon-nucleon potential with charge-independence breaking. Phys. Rev. C **51**, 38 (1995). https://doi.org/10.1103/PhysRevC.51.38
62. A. Gezerlis, I. Tews, E. Epelbaum et al., Quantum Monte Carlo calculations with chiral effective field theory interactions. Phys. Rev. Lett. **111**, 032501 (2013). https://doi.org/10.1103/PhysRevLett.111.032501
63. A. Roggero, A. Mukherjee, F. Pederiva, Quantum Monte Carlo calculations of neutron matter with nonlocal chiral interactions. Phys. Rev. Lett. **112**, 221103 (2014). https://doi.org/10.1103/PhysRevLett.112.221103
64. J.E. Lynn, J. Carlson, E. Epelbaum et al., Quantum Monte Carlo calculations of light nuclei using chiral potentials. Phys. Rev. Lett. **113**, 192501 (2014). https://doi.org/10.1103/PhysRevLett.113.192501
65. M. Piarulli, L. Girlanda, R. Schiavilla et al., Minimally nonlocal nucleon-nucleon potentials with chiral two-pion exchange including Δ resonances. Phys. Rev. C **91**, 024003 (2015). https://doi.org/10.1103/PhysRevC.91.024003
66. M. Piarulli, L. Girlanda, R. Schiavilla et al., Local chiral potentials with Δ-intermediate states and the structure of light nuclei. Phys. Rev. C **94**, 054007 (2016). https://doi.org/10.1103/PhysRevC.94.054007
67. D. Lonardoni, S. Gandolfi, J.E. Lynn et al., Auxiliary field diffusion Monte Carlo calculations of light and medium-mass nuclei with local chiral interactions. Phys. Rev. C **97**, 044318 (2018). https://doi.org/10.1103/PhysRevC.97.044318
68. D. Lonardoni, I. Tews, S. Gandolfi et al., Nuclear and neutron-star matter from local chiral interactions. Phys. Rev. Res. **2**, 022033 (2020). https://doi.org/10.1103/PhysRevResearch.2.022033
69. B.S. Pudliner, V.R. Pandharipande, J. Carlson et al., Quantum Monte Carlo calculations of nuclei with $A \leq 7$. Phys. Rev. C **56**, 1720 (1997). https://doi.org/10.1103/PhysRevC.56.1720
70. R.B. Wiringa, S.C. Pieper, Evolution of nuclear spectra with nuclear forces. Phys. Rev. Lett. **89**, 182501 (2002). https://doi.org/10.1103/PhysRevLett.89.182501
71. D. P. Kingma, J. Ba, Adam: A Method for Stochastic Optimization, in *booktitle 3rd International Conference on Learning Representations, ICLR 2015, San Diego, CA, USA, May 7-9, 2015, Conference Track Proceedings*, edited by Y. Bengio and Y. LeCun (2015) arXiv:1412.6980 [cs.LG]
72. M. Abadi, A. Agarwal, P. Barham et al., TensorFlow: Large-scale machine learning on heterogeneous systems (2015). https://www.tensorflow.org/
73. C. A. Bertulani, *Nuclear Physics in a Nutshell* (Princeton University Press, Princeton, New Jersey, 2007)
74. https://www.phy.anl.gov/theory/research/av18/
75. W.J. Huang, M. Wang, F.G. Kondev et al., The AME 2020 atomic mass evaluation (I). Evaluation of input data, and adjustment procedures. Chin. Phys. C **45**, 030002 (2021). https://doi.org/10.1088/1674-1137/abddb0
76. M. Wang, W.J. Huang, F.G. Kondev et al., The AME 2020 atomic mass evaluation (II). Tables, graphs and references. Chin. Phys. C **45**, 030003 (2021). https://doi.org/10.1088/1674-1137/abddaf
77. H. Robbins, S. Monro, A stochastic approximation method. Ann. Math. Statist. **22**, 400 (1951). https://doi.org/10.1214/aoms/1177729586
78. E. Nielsen, D.V. Fedorov, A.S. Jensen et al., The three-body problem with short-range interactions. Phys. Rep. **347**, 373 (2001). https://doi.org/10.1016/S0370-1573(00)00107-1
79. C. Wang, T. Naito, J. Li et al., A deep neural network approach to solve the Dirac equation. Eur. Phys. J. A **61**, 162 (2025). https://doi.org/10.1140/epja/s10050-025-01630-5